Mapping an on-chip terahertz antenna by a scanning near-field probe and a fixed field-effect transistor*

Lü Li(吕 利)[a)b)], Sun Jian-Dong(孙建东)[a)†], Roger A. Lewis[c)], Sun Yun-Fei(孙云飞)[d)], Wu Dong-Min(吴东岷)[a)d)], Cai Yong(蔡 勇)[a)], and Qin Hua(秦 华)[a)‡]

[a)] *Key Laboratory of Nanodevices and Applications, Suzhou Institute of Nano-tech and Nano-bionics, Chinese Academy of Sciences, Suzhou* 215123, *China*
[b)] *Graduate University of Chinese Academy of Sciences, Beijing* 100049, *China*
[c)] *Institute for Superconducting and Electronic Materials and School of Physics, University of Wollongong, Wollongong, New South Wales* 2522, *Australia*
[d)] *i-Lab, Suzhou Institute of Nano-tech and Nano-bionics, Chinese Academy of Sciences, Suzhou* 215123, *China*

(Received 16 August 2014; revised manuscript received 23 September 2014; published online 10 December 2014)

In the terahertz (THz) regime, the active region for a solid-state detector usually needs to be implemented accurately in the near-field region of an on-chip antenna. Mapping of the near-field strength could allow for rapid verification and optimization of new antenna/detector designs. Here, we report a proof-of-concept experiment in which the field mapping is realized by a scanning metallic probe and a fixed AlGaN/GaN field-effect transistor. Experiment results agree well with the electromagnetic-wave simulations. The results also suggest a field-effect THz detector combined with a probe tip could serve as a high sensitivity THz near-field sensor.

Keywords: terahertz detector, terahertz antenna, near-field probe, high electron mobility transistor

PACS: 85.60.Gz, 72.80.Ey, 87.50.U–, 87.64.mt **DOI:** 10.1088/1674-1056/24/2/028504

1. Introduction

In the terahertz (THz, 1 THz = 10^{12} Hz) portion of the electromagnetic spectrum, many sensing applications, such as security screening, near-field microscopy, and spectroscopy, are being studied and developed.[1] Sensitive detectors are one of the key elements for such applications.[2] In various THz detectors, antennas are commonly applied to feed incident THz electromagnetic (EM) radiation into the active region of the detectors.[3–9] The efficiency of these antennas is crucial for high sensitivity and is largely determined by the near-field properties. The near-field distribution is usually obtained by performing a finite-element analysis of the EM wave.[10–13] From the point of view of detector optimization/development, it would be beneficial to experimentally obtain the near-field distribution. In many THz near-field experiments/applications, the near-field EM wave is transferred by either a sharpened metallic probe tip or by a metallic pinhole aperture into the far field and detected therein.[14–17] In THz time-domain spectroscopy, a photoconductive detector has been integrated on a probe tip and serves as a direct near field THz detector.[18] Here, we report our experiment on imaging the near-field response of an antenna-coupled field-effect-transistor (FET) THz detector by scanning the antennas using a sharpened metallic tip. In the experiment, the scanning metallic tip serves as a near-field coupler/agitator of the antennas and the integrated FET detector reads out the THz intensity. The experimental results are in good agreement with a finite-difference time-domain (FDTD) simulation. This method allows us to experimentally distinguish the most effective antenna blocks and provides direct guidance for the optimization of antennas and detectors.

2. Experiment

The experimental setup is schematically shown in Fig. 1(a), where the THz radiation from a backward wave oscillator (BWO) is collected, collimated, and focused by a pair of off-axis parabolic mirrors (OAP#1 and OAP#2). The THz frequency is set at $f_0 = 875$ GHz corresponding to a free-space wavelength of $\lambda_0 = 343$ μm. The schematic zoom-in view of the metallic probe scanning the detector surface is shown in Fig. 1(b). The THz wave is polarized in direction x. The metallic probe is glued on a piezoelectric vibrator which is driven by a sinusoidal voltage with frequency 123 Hz and peak-to-peak voltage 5 V. The probe tip vibrates in direction x and the vibration amplitude is $\delta x_p \approx 1$ μm. Accurate positioning and raster scanning of the probe tip at a certain distance to the detector surface are realized by mounting the piezoelectric vibrator on a step-motorized XYZ stage. The probe is made of tungsten and, as shown in Fig. 1(c), has a diameter of 500 μm. The

*Project partially supported by the Knowledge Innovation Program of the Chinese Academy of Sciences (Grant No. KJCX2-EW-705), China Postdoctoral Science Foundation (Grant No. 2014M551678), Jiangsu Planned Projects for Postdoctoral Research Funds (Grant No. 1301054B), Instrument Developing Project of the Chinese Academy of Sciences (Grant No. YZ201152), the National Natural Science Foundation of China (Grant No. 61271157), Suzhou Science and Technology Project (Grant No. ZXG2012024), and the Chinese Academy of Sciences Visiting Professorship for Senior International Scientists (Grant No. 2010T2J07).

†Corresponding author. E-mail: dsun2008@sinano.ac.cn
‡Corresponding author. E-mail: hqin2007@sinano.ac.cn

© 2015 Chinese Physical Society and IOP Publishing Ltd

radius of the probe tip is sharpened to about 0.5 μm by electrochemical etching in NaOH solution. The detector is similar to that reported earlier by Sun *et al.*[3] A partial top view of the detector is shown in Fig. 1(d). The active electron channel is made of the two-dimensional electron gas (2DEG) from an AlGaN/GaN heterostructure and the width in direction y is $W = 10$ μm. The antenna contains three blocks (A, B, and C). Each block is 45-μm long in direction x and maximally 14-μm wide in direction y. Only block C is directly connected to the external electronics via the electrode for applying the gate voltage. Blocks A and B are capacitively coupled to the 2DEG channel. The gate in the center of the detector controls the electron density underneath and has a length of $L = 2$ μm in direction x. The Ohmic contacts for the 2DEG channel are about 100 μm away from the gate. The sapphire substrate of the detector is transparent for the incident THz wave and is thinned to 200 μm. A high resolution-power microscope is used to monitor the probe tip and the THz detector. The net photocurrent induced by the vibrating probe is amplified by a current preamplifier, and then read out by a lock-in amplifier. By raster scanning the probe tip at distance z_p to the detector surface, the tip-induced photocurrent can be mapped as a function of the tip location (x_p, y_p).

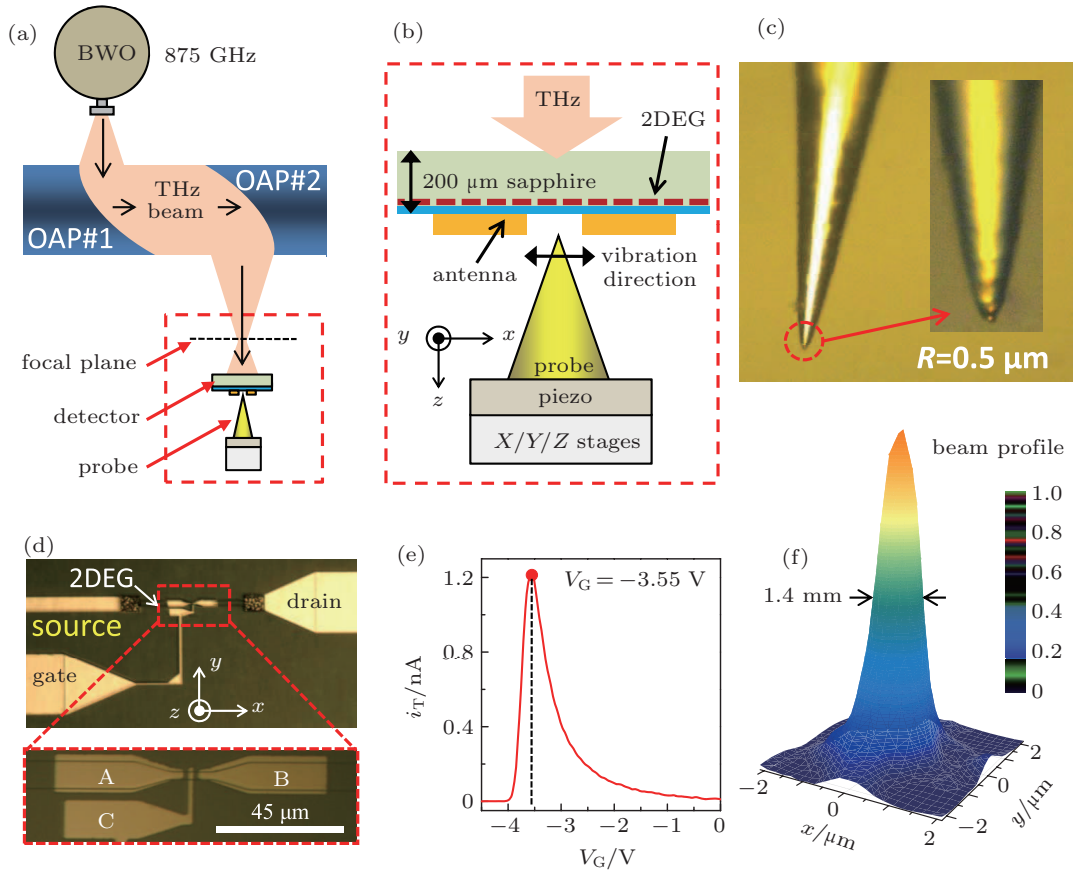


Fig. 1. (color online) (a) Schematics of the experiment setup. The continuous-wave THz source is tuned at 875 GHz. (b) Zoom-in view of the near-field probing scheme by using a motorized vibrating probe. (c) Optical microscope images of the metallic probe and the tip. (d) Optical microscope image of the field-effect THz detector. The zoom-in box shows the central active region including three antenna blocks (A, B, C), the gate, and the two-dimensional electron gas (2DEG) channel. (e) The photocurrent (i_T) tuned by the gate voltage (V_G). (f) The THz beam profile probed by the detector scanned in the focal plane of OAP#2.

3. Characterization and discussion

The detector was first characterized by measuring the photocurrent without the probe tip upon THz irradiation of $f_0 = 875$ GHz. The photocurrent (i_T) as a function of the gate voltage (V_G) is shown in Fig. 1(e). The peak photoresponse is located at $V_G = -3.55$ V. For the following experiments, the gate voltage is fixed at this optimal value. The profile of the THz beam, as shown in Fig. 1(f), was obtained by raster scanning the detector in the focal plane of OAP#2 with a step size of 50 μm. The minimum beam width is about 1.4 mm and is about 15 times larger than the overall antenna dimension (≈ 90 μm) in direction x. In the following experiments, the detector is moved slightly away from the focal plane so that the whole antenna area is under a uniform irradiation, as schematically shown in Fig. 1(a).

A photocurrent image as shown in Fig. 2(a) was obtained

by scanning the tip with $z_p = 0.5$ μm. The antenna profile is overlaid on the map for easy pattern recognition. Each antenna block shows a different THz response to the scanning tip. The maximum response is observed at $(x_p, y_p) = (25$ μm, 0 μm), i.e., at the center of antenna block B. When the probe tip is located near the center of antenna block C, a weaker, but yet significant, photocurrent is observed. In comparison to antenna blocks B and C, the vibrating probe tip above antenna block A induces a much weaker photocurrent. The signal-to-noise ratio is only 2.7 corresponding to the noise floor of 1.5 pA. For clarity, two line scans along direction x and one scan along direction y were extracted from Fig. 2(a). The corresponding locations of these scans are marked by the dash–dotted ($y_p = 0$ μm), dashed ($y_p = -17.5$ μm), and dash–dot–dotted line ($x_p = 25$ μm) in Fig. 2(a) and plotted in Figs. 2(b)–2(d). The line scan at $y_p = 0$ μm, crossing both antennas A and B, is shown in Fig. 2(b). Two peaks at $x_p \approx \pm 25$ μm are clearly identified corresponding to the center points of antenna A and antenna B, respectively. The full-width-at-half-maximum (FWHM) of the peak originated from antenna B is about 30 μm, corresponding to a spatial resolution about $\lambda_0/11$, which is slightly smaller than the antenna width in direction y. The line scan at $y_p = -17.5$ μm, crossing only antenna C, is shown in Fig. 2(c). Two peaks with a similar amplitude are shown clearly. The line scan at $x_p = 25$ μm crossing antenna B is shown in Fig. 2(d). The FWHM in direction y is about 40 μm, slightly smaller than the antenna width in direction y and slightly larger than the FWHM in direction x.

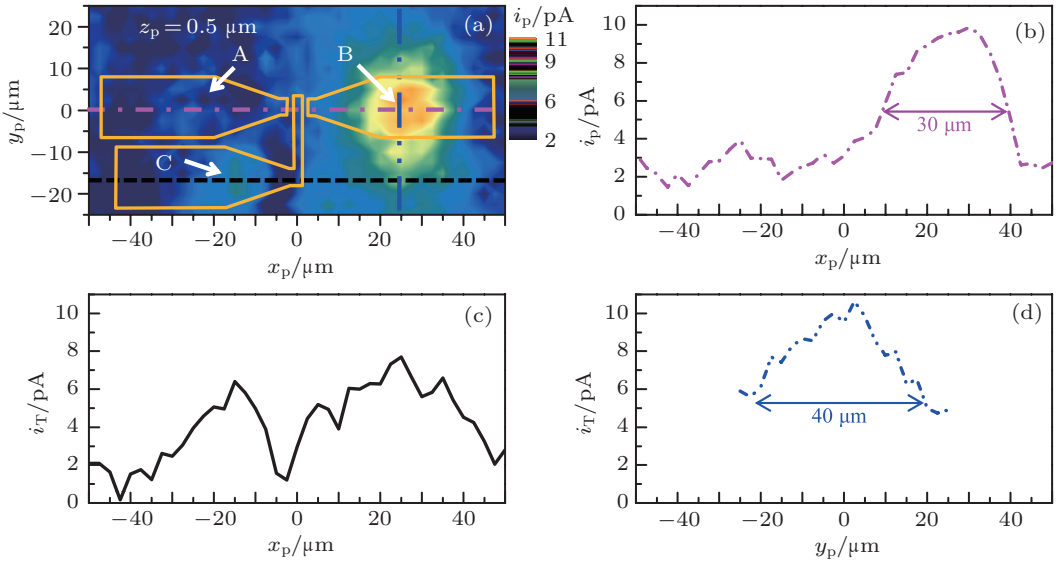


Fig. 2. (color online) (a) Map of the tip-induced photocurrent (i_p) by raster scanning the tip with a tip-detector distance of $z_p = 0.5$ μm. The profile of the antennas and the gate is overlaid on the map. (b) A line scan along the dash–dotted line in panel (a), i.e., with $y_p = 0$ μm. (c) A line scan along the dashed line in panel (a), i.e., with $y_p = -17.5$ μm. (d) A line scan along the dash–dot–dotted line in panel (a), i.e., with $x_p = 25$ μm.

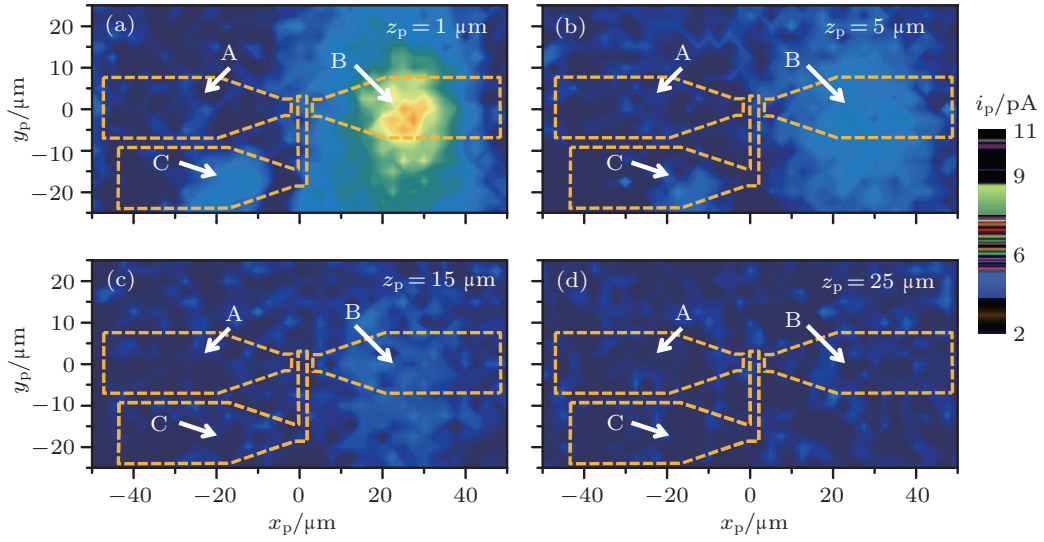


Fig. 3. (color online) Maps of the tip-induced photocurrent by raster scanning the tip at different tip-detector distances: (a) $z_p = 1$ μm, (b) $z_p = 5$ μm, (c) $z_p = 15$ μm, and (d) $z_p = 25$ μm.

With a tip-antenna distance of $z_p = 0.5$ μm, different roles of three antenna blocks can be roughly identified as the ones shown in Fig. 2(a). The tip-induced photocurrent was further examined at larger tip-detector distances. As shown in Figs. 3(a)–3(d), four raster scans were obtained with $z_p = 1$, 5, 15, and 25 μm, respectively. We found that the smaller the tip-detector distance, the stronger the photocurrent. When the tip-detector distance is greater than 15 μm, the detector becomes very insensitive to the probe tip. At a distance of 25 μm, the induced photocurrent is submerged in the background noise. There is an inactive region near the right-angle bend of antenna C, where a minimum photocurrent is observed. This feature clearly confirms that antenna B and antenna C have opposite polarizations.

The interaction between the tip and antenna block B was further examined by probing the photocurrent as a function of distance z_p when the tip is pointed to the center of antenna B. As shown in Fig. 4(a), by moving the probe tip away from antenna block B to a distance about 10 μm $\approx \lambda/34$, the photocurrent decreases abruptly indicating a near-field interaction mechanism. On further increasing the distance, an oscillation in the photocurrent was observed. A minimum occurs at $z_p = 46$ μm $\approx \lambda/7.5$ and a maximum occurs at $z_p = 86$ μm $\approx \lambda/4$.

According to the detection mechanism,[10] the THz photocurrent is proportional to the integral of the local mixing factor ($\eta = \dot{\xi}_x \dot{\xi}_z \cos(\phi)$), the incident THz power flux (P_0), and the extent of electron density tuned by the gate voltage ($\mathrm{d}n/\mathrm{d}V_G$): $i_T = \alpha \int_0^L \eta \mathrm{d}x$, where $\alpha = (e\mu W Z_0 P_0 \bar{z}/2L)\mathrm{d}n/\mathrm{d}V_G$, e is the elementary charge, μ is the electron mobility, n is the electron density of the 2DEG, Z_0 is the free-space impedance, and $\bar{z}$ is an effective distance between the antenna and the 2DEG.[10] Factors $\dot{\xi}_x$ and $\dot{\xi}_z$ correspond to the THz field enhancement in directions x and z. Phase ϕ is the phase difference between the two field components. Vibrating the probe tip in direction x modulates the local THz electric fields and hence the mixing factor. Although the specific manner of how the tip alters the THz field is unknown, we can model the tip-induced photocurrent as

$$i_p = \frac{\mathrm{d}i_T}{\mathrm{d}x_p} \times \delta x_p = \delta x_p \times \alpha \int_0^L \frac{\mathrm{d}\eta}{\mathrm{d}x_p} \mathrm{d}x. \quad (1)$$

In order to obtain insight into the mechanism of the tip-antenna interaction, finite-difference-time-domain (FDTD) simulations were performed to determine the differences in the mixing factor depending on whether the tip is present or not, as shown in Fig. 4(b). The simulation result suggests that mixing occurs predominately around $x_c = \pm 1$ μm, i.e., near the edges of the gated 2DEG channel. Furthermore, the mixing factor at $x_c = +1$ μm is greater than that at $x_c = -1$ μm. The simulation also suggests that the near-field tip coupled to antenna block B enhances the mixing factor by 46% and 19.6% at $x_c = -1$ μm and at $x_c = +1$ μm, respectively. This confirms that the antennas predominately determine the mixing factors and the probe tip induces only a perturbation. Since it requires a huge mesh to simulate the detector-tip configuration, it is not practical to make a full simulation of term $\mathrm{d}\eta/\mathrm{d}x_p$. Nevertheless, simulations of the mixing factor as a function of the tip-antenna distance were performed. The simulated data points in an arbitrary unit are overlaid on the experimental tip-induced photocurrent as shown in Fig. 4(a). Both the near-field response and the interference effect are recovered. However, there is a remarkable deviation between the simulation and the experimental data when $z_p < 60$ μm, i.e., within the near-field zone. The deviation is most probably from the insufficient mesh number in the simulation since the near-field property is very sensitive to the distance and the shape of the tip.

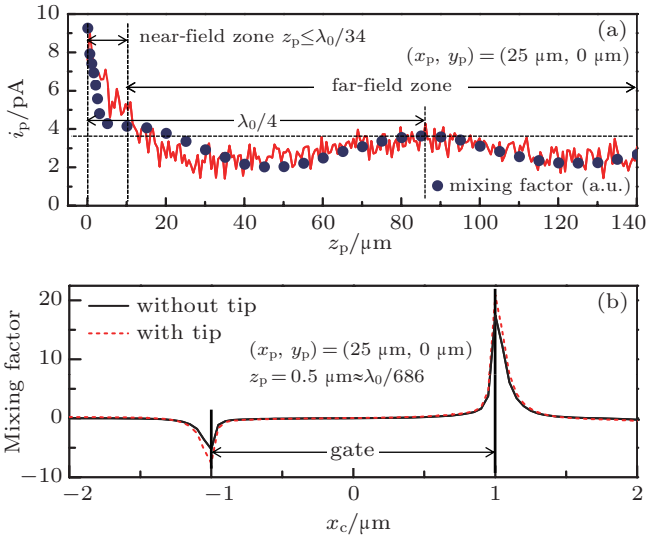


Fig. 4. (color online) (a) Tip-induced photocurrent as a function of the tip-antenna distance. The tip is pointed to the center of antenna block B, i.e., at (x_p, x_y)=(25 μm, 0 μm). The solid data points in an arbitrary unit are simulated mixing factors at $x_c = 1$ μm. (b) Simulated mixing factors in the 2DEG channel with and without the near-field probe tip. In both simulations, the probe-antenna distance is set at $z_p = 0.5$ μm.

From the raster scans shown in Fig. 2(a) and Fig. 3, we infer that block B is the most effective part of the THz antenna and the other two blocks are complementary. Our experiment also suggests that a THz near-field sensor maybe constructed by integrating a sharp metallic tip with antenna B. In this way, the tip serves as a scanning near-field antenna, antenna block B serves as a THz transmission line, and the gate controlled field-effect channel functions as a sensitive detector. Such an integrated near-field sensor may provide a simple solution for THz microscopy with high resolving power.

In the current experiment, the tip vibrates in direction x and the vibration amplitude is much less than the antenna dimension. The antenna is less sensitive to the location of the tip than to the tip-antenna distance. According to the simulation shown in Fig. 4(b), a tip vibrating in the z direction would allow for more straightforward probing of the near-field effect.

For this reason, a modified probe system using a quartz tuning fork to excite the tip vibration in the z direction is under development. This system may allow for spontaneous imaging of the detector morphology in the atomic-force-microscopy mode.

4. Conclusions

In conclusion, we have performed a near-field imaging experiment on an antenna-coupled field-effect THz detector. The combined use of a scanning metallic probe and the field-effect THz detector allowed us to image the active region of THz antennas. This method provides an alternative way for rapid verification of THz antenna design. Furthermore, an integrated scanning THz sensor may be developed for high-resolution THz microscopes.

References

[1] Sizov F and Rogalski A 2010 *Progress in Quantum Electronics* **34** 278
[2] Tonouchi M 2007 *Nat. Photon.* **1** 97
[3] Sun J D, Sun Y F, Wu D M, Cai Y, Qin H and Zhang B S 2012 *Appl. Phys. Lett.* **100** 013506
[4] Sun Y F, Sun J D, Zhang X Y, Qin H, Zhang B S and Wu D M 2012 *Chin. Phys. B* **21** 108504
[5] Tanigawa T, Onishi T, Takigawa S and Otsuji T 2010 *Device Research Conference (DRC)*, South Bend, June 22, 2010, p. 167
[6] Lisauskas A, Mundt M, Seliuta D, Minkevicius L, Kasalynas I, Valusis G, Mittendorff M, Winnerl S, Krozer V and Roskos H G 2012 *IEEE Trans. Microwave Theory* **60** 3834
[7] Vicarelli L, Vitiello M S, Coquillat D, Lombardo A, Ferrari A C, Knap W, Polini M, Pellegrini V and Tredicucci A 2012 *Nat. Mater.* **11** 865
[8] Dyer G C, Vinh N Q, Allen S J, Aizin G R, Mikalopas J, Reno J L and Shaner E A 2010 *Appl. Phys. Lett.* **97** 193507
[9] Kim S, Zimmerman J D, Focardi P, Gossard A C, Wu D H and Sherwin M S 2008 *Appl. Phys. Lett.* **92** 253508
[10] Sun J D, Qin H, Lewis R A, Sun Y F, Zhang X Y, Cai Y, Wu D M and Zhang B S 2012 *Appl. Phys. Lett.* **100** 173513
[11] Deibel J A, Escarra M, Berndsen N, Wang K and Mittleman D M 2007 *Proc. IEEE* **95** 1624
[12] Chen H T, Padilla W J, Zide J M, Gossard A C, Taylor A J and Averitt R D 2006 *Nature* **444** 597
[13] Yang K, David G, Yook J G, Papapolymerou I, Katehi L P, Whitaker J F 2000 *IEEE Trans. Microwave Theory* **48** 288
[14] Rosner B T and van der Weide D W 2002 *Rev. Sci. Instrum.* **73** 2505
[15] Chen H T, Kersting R and Cho G C 2003 *Appl. Phys. Lett.* **83** 3009
[16] Mitrofanov O, Bener I, Harel R, Wynn J D, Pfeiffer L N, West K W and Federici J 2000 *Appl. Phys. Lett.* **77** 3496
[17] Mitrofanov O, Lee M, Hsu J W, Pfeiffer L N, West K W, Wynn J D and Federici J F 2001 *Appl. Phys. Lett.* **79** 907
[18] Kawano Y and Ishibashi K 2008 *Nat. Photon.* **2** 618